Machine vision system for on-line wholesomeness inspection of poultry carcasses[1]

C.-C. Yang,* K. Chao,*[2] M. S. Kim,* D. E. Chan,* H. L. Early,†[3] and M. Bell‡

*Environmental Microbial and Food Safety Laboratory, USDA-Agricultural Research Service, Building 303, BARC-East, Powder Mill Road, Beltsville, MD 20705; †Food Safety and Inspection Service, USDA, Washington, DC 20705; and ‡Stork Food Systems, 1024 Airport Parkway, Gainesville, GA 30501

ABSTRACT A line-scan machine vision system and multispectral inspection algorithm was developed and evaluated for differentiation of wholesome and systemically diseased chickens on a high-speed processing line. The inspection system acquires line-scan images of chicken carcasses on a 140 bird/min processing line and is able to automatically detect individual birds entering and exiting the field of view of the camera, locate a specified region of interest for spectral image analysis, and produce a decision output for each bird. The same spectral line-scan imaging system was used for hyperspectral data acquisition-analysis to develop the multispectral detection and differentiation algorithm and for multispectral implementation of the algorithm for real-time on-line inspection on the processing line. Results showed that effective multispectral inspection could be achieved by analysis of a selected region of interest across the breast area from images at the 580- and 620-nm wavebands. Overall system performance was evaluated during two 8-h shifts in which the system inspected over 100,000 chickens, with system results compared with Food Safety and Inspection Service inspector tallies of wholesome and systemically diseased birds for that same time period. During system verification, the system accurately classified wholesome and systemically diseased chickens that were observed by a veterinarian posted beside the system to perform real-time identifications of the same birds. The high accuracy of the results demonstrated that the spectra line-scan imaging system and multispectral detection and differentiation algorithm can be effectively used for on-line high-speed presorting applications for young broiler chickens.

Key words: food safety, poultry inspection, spectral imaging, line scan

2010 Poultry Science 89:1252–1264
doi:10.3382/ps.2008-00561

INTRODUCTION

American chicken plants processed almost 9 billion broiler chickens in 2008 (USDA, 2009). To help maintain product safety and reduce the risk of food safety hazards for poultry, egg, and meat products, the USDA Food Safety and Inspection Service (**FSIS**) implemented the Hazard Analysis and Critical Control Point program in processing plants throughout the country (USDA, 1996) and, more recently, has been testing the Hazard Analysis and Critical Control Point-Based Inspection Models Project (**HIMP**) in a small number of volunteer plants (USDA, 1997). The HIMP performance standards require that chickens with infectious conditions such as septicemia and toxemia be removed from the processing lines. Processing plants seeking to satisfy increasing consumer demand by increasing their output through faster processing speeds are limited by the current inspection system, which limits each human inspector on the line to examining a maximum of 35 birds/min. New high-speed inspection technologies may help poultry plants to maintain their competitiveness and increase production throughput while ensuring that food safety regulations are satisfied.

Effective automated imaging inspection systems must be able to effectively acquire and process images of carcasses at the high speeds of commercial processing lines. Previous work to develop imaging technologies suitable for commercial processing has included systems and methods targeting poultry processing control and management (Daley et al., 2003; Usher et al., 2005) and automated food safety inspection for contamination detection and carcass wholesomeness (Park and Chen, 1996; Lawrence et al., 2003b; Yang et al.,

Received December 23, 2008.
Accepted February 15, 2010.
[1]Mention of company or trade names is for descriptive purposes only and does not imply endorsement or approval by the USDA to the exclusion of other products that may be suitable.
[2]Corresponding author: kevin.chao@ars.usda.gov
[3]Retired.

2006b). In particular, the combined advantages of machine vision and spectroscopy-based analysis are realized with spectral imaging methods that can produce high accuracy in automated applications. Nondestructive multispectral imaging shows great potential for high-speed on-line inspection for commercial processing lines; the acquisition of both spectral and spatial information from bird surfaces allows for efficient and accurate evaluation of both quality and safety criteria, such as systemic or localized disease conditions, contamination detection, and quality traits such as bird size, defects, and damage.

Multispectral imaging relies on the selection of several key imaging wavebands. With spatially matched images at several wavelengths, analysis algorithms can include a variety of pixel-based arithmetic methods, such as band ratios and differences, as well as conventional machine vision techniques, resulting in enhanced spectral- and spatial-based image features that are useful for rapid and effective inspection applications. Both spectral and spatial features are critical to effective on-line poultry inspection, as demonstrated by several recent laboratory and pilot-scale studies. Yang et al. (2005) achieved classification accuracies of 95.7% for wholesome and 97.7% for unwholesome (systemically diseased) chicken carcasses using multispectral images at the 540-, 610-, and 700-nm wavebands. Park et al. (2002) achieved 97.3 to 100% accuracies in identifying fecal and ingesta contamination of poultry carcasses using images at the 434-, 517-, 565-, and 628-nm wavebands.

A primary factor for effective multispectral imaging inspection is the selection of wavebands appropriate to the application at hand (Mehl et al., 2002; Windham et al., 2003). In the past, conventional development of on-line multispectral methods often used spectroscopy analysis or hyperspectral imaging analysis in the laboratory to first select specific wavebands useful for the identification of a particular disease, contamination, or defect problem. Once specific wavebands and image features were determined, it was usually necessary to implement these wavebands and features using interference filters on a separate camera system suitable for on-line multispectral inspection. Thus, a major challenge of this conventional approach was the difficulty of cross-system calibration to transfer the imaging settings, developed by a spectrophotometer or hyperspectral imaging system, to a separate filter-based multispectral imaging system (Lawrence et al., 2003a). Considerable effort was required to ensure that the final multispectral imaging system, utilizing different optical components, would produce the same results as the spectrophotometer or hyperspectral imaging equipment used during system development.

Some recent studies have overcome the challenges of cross-system calibration by using a hyperspectral-multispectral line-scan machine vision system for system development through hyperspectral analysis to determine waveband selection and then using the same camera system to implement on-line multispectral inspection (Yang et al., 2006a; Chao et al., 2007). This system uses an imaging spectrograph to continuously acquire narrow line-scan images across a linear field of view (**FOV**) while moving targets across the FOV. In hyperspectral imaging mode, full-spectrum data are acquired for each pixel in every line-scan image. Algorithms to process the line-scan images can thus compile complete images of the target objects and perform both spectral and spatial analysis for determining wavebands and image features for multispectral inspection purposes. The same system can then be used in multispectral mode, using only the specific wavebands and image features selected. By acquiring only selected wavebands for every pixel instead of full-spectrum data, the volume of spectral data to be analyzed is reduced and on-line multispectral imaging can then be performed with high accuracy for objects moving at very high speeds.

The objective of this paper is to describe the development, validation, and evaluation of a line-scan spectral imaging system for on-line inspection of wholesome and unwholesome (systemically diseased) chickens on a commercial high-speed processing line. A line-scan algorithm was developed and implemented for the system to automatically detect each new bird on the line, to identify image pixels to be analyzed for each bird, and to classify each bird as wholesome or unwholesome immediately after the bird exits the FOV and before the next bird appears. Overall system performance on a commercial chicken kill line operating at 140 birds/min was evaluated by verification against a veterinarian's bird identifications and also by comparison of the inspection system's results with tallies produced by human inspectors after two 8-h shifts in the chicken processing plant.

MATERIALS AND METHODS

Line-Scan Machine Vision System

The design of the line-scan machine vision system was based on the use of an electron-multiplying charge-coupled-device camera and an imaging spectrograph with a linear FOV created by a slit in front of the spectrograph. The FOV was illuminated by 2 pairs of high-power, broad-spectrum white light-emitting-diode (**LED**) line lights (LL6212, Advanced Illumination Inc., Rochester, VT). A collimated light beam from each pixel of the scanned line was dispersed through the ImSpectro V10 spectrograph (Spectral Imaging Ltd., Oulu, Finland) to obtain a spectrum; therefore, a 2-dimensional image of reflectance intensity was acquired for each scanned line with spatial position along one axis (spatial dimension) and spectral waveband along the other (spectral dimension). The PhotonMax 512b electron-multiplying charge-coupled-device camera (Princeton Instruments, Roper Scientific Inc., Trenton, NJ) used thermoelectric cooling of its 512 × 512 pixel detector array to an operating temperature of −70°C and was used with a

10-MHz, 16-bit digitizer for high-speed, low-light image acquisition. The inspection software was built on a LabVIEW 8.2 (National Instruments, Austin, TX) platform.

As shown in Figure 1, the distance from the camera lens to the shackle line was 914 mm. The angles of illumination before and after the linear FOV were adjusted to maximize the reflectance intensity. Two line lights were mounted together on a single joint to the right of the camera, such that their angles of illumination were not independently adjustable. The other 2 line lights were similarly mounted to the left of the camera. The right pair and the left pairs were separated by 115 mm, each pair at a distance of 254 mm perpendicular to the shackle line (measured from shackle line to mounting joint). The inner pair of line lights was positioned slightly behind the outer pair rather than with their forward faces flush, to allow for some forward movement of the target surface (up to 25 mm) so that the convex surface of a bird, even if pushed slightly more forward than normal, would still be adequately and uniformly illuminated. The outer pair was positioned a half head lower than the inner pair to avoid the interference that would have resulted if the adjacent LED lights had been mounted at equal height. The vertical FOV for each scanned line was 178 mm. The spatial resolution of each line-scan image was 0.35 × 0.35 mm per pixel.

As described above, a single line-scan image covers a linear spatial FOV of 178 mm in height. This linear distance was represented by 512 spatial points. By default, the 512 × 512 detector array can acquire a single hyperspectral line-scan image consisting of 512 spectral data points for each of the 512 spatial points—a total image size of 512 × 512 pixels. This line-scan image size was reduced by binning the spectral dimension by 4 (i.e., accumulating every 4 pixels along the spectral dimension as 1 pixel, thereby reducing the total line-

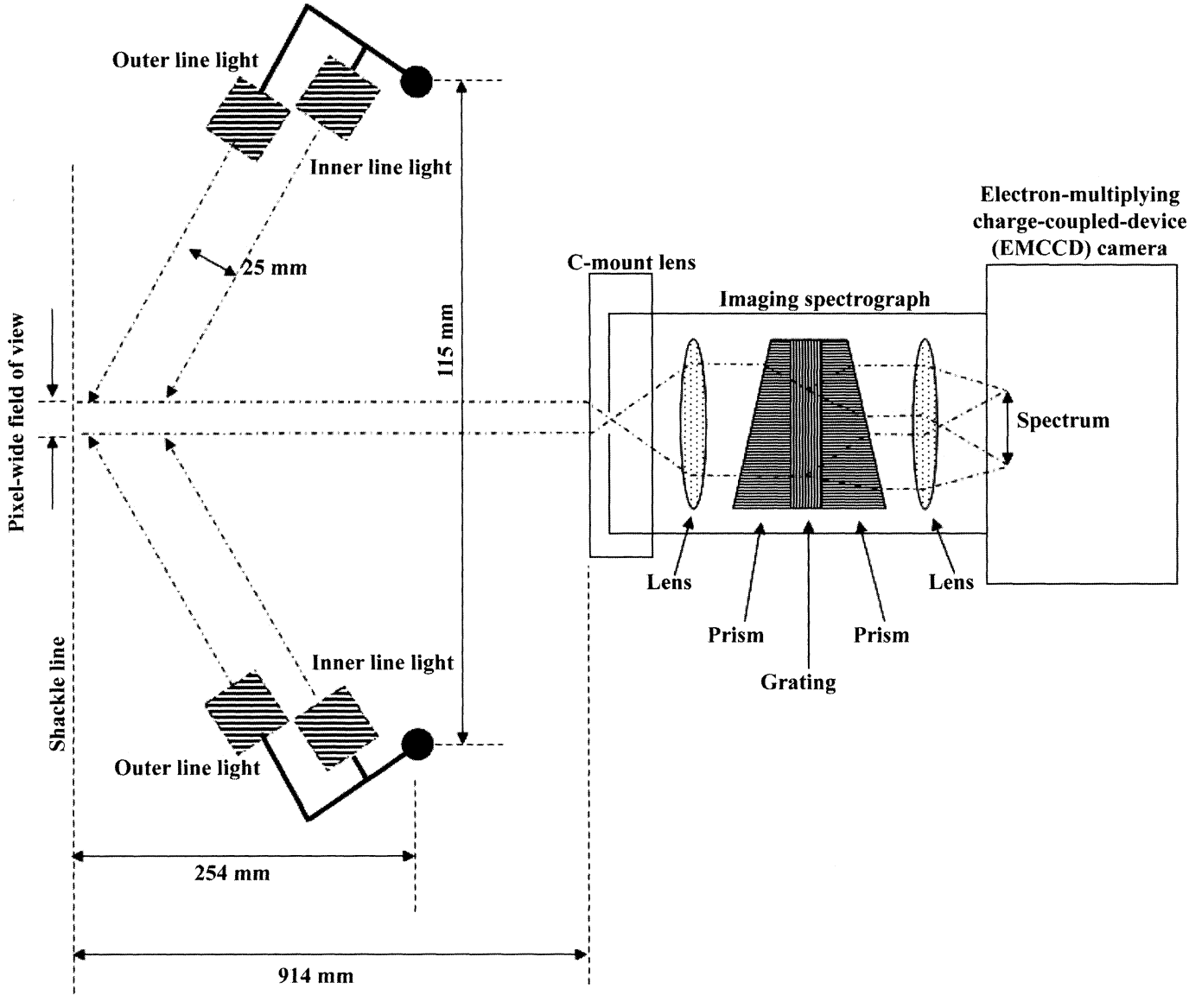

Figure 1. Schematic of spectral imaging system and illumination position on processing line.

scan image size to 512 × 128 pixels). With the LED line lights illuminating a 99% diffuse reflectance target (Spectralon, Labsphere, North Sutton, NH), it was observed that for the first 19 spectral channels and the last 54 spectral channels (out of 128 total), the reflectance from the LED lights was too low to be useful. These channels were consequently discarded and all hyperspectral imaging was performed using only the remaining 55 spectral channels (512 × 55 pixels). Spectral calibration performed using 6 spectral peaks from the emission of a neon-mercury pencil light: 436 and 546 nm from mercury and 614, 640, 703, and 724 nm from neon. The 55 channels of each hyperspectral line-scan image spanned from 389 to 744 nm, respectively, with an average spectral bandwidth of 6.6 nm.

During real-time continuous operation, the spectral line-scan imaging system can immediately analyze each line-scan as it is acquired and also analyze a set of line-scan images compiled for one target (such as one whole bird) before the next target enters the FOV. The significant advantage presented by this system is its capacity to continuously operate in either hyperspectral or multispectral mode, with the ability to select any of the available spectral channels through the camera control software. As described above, each hyperspectral line-scan image acquired in this study consisted of spectral data across 55 spectral channels (after binning) for each spatial point in the line-scan image. Hyperspectral analysis was performed to select wavebands and develop inspection algorithms for multispectral inspection of chickens for wholesomeness using the same imaging system; implementation of the selected wavebands would thus only involve adjustments through software control settings, rather than implementation of optical filters on an entirely separate imaging system as might be required for conventional multispectral imaging systems.

During system development, the wavebands essential for differentiation of wholesome and systemically diseased chickens were selected from analysis of the hyperspectral images. For on-line differentiation of poultry carcasses, only measurements for the spectral pixels corresponding to the selected wavebands were digitized for the computer and used by the system in multispectral imaging mode. Both hyperspectral and multispectral line-scan images in this study were acquired using a camera exposure time of 0.1 ms with an electron-multiplying gain of 45. This short exposure time was critical to the effective performance of the system for on-line imaging inspection of chicken carcasses on the rapidly moving processing line.

Overview of 3-Stage Experiment

This work to develop and test a multispectral imaging-based method to differentiate wholesome and systemically diseased chickens was performed in 3 stages. In stage I, hyperspectral line-scan images of chickens on the processing line were acquired on-line and then compiled and analyzed in the laboratory to develop specific waveband and image feature selections for use in multispectral inspection. In stage II, validation of the waveband and image feature selections was performed by repeating the waveband and image feature selection process using a new set of hyperspectral images acquired on-line in the processing plant. Validation was also performed by using the selected wavebands and image features during on-line multispectral inspection in the processing plant and comparing the imaging system's results with a limited number of bird evaluations performed by a veterinarian observing the same birds as they passed on the processing line. In stage III, the performance of the imaging system was evaluated based on continuous multispectral inspection of chickens during two 8-h shifts in the processing plant.

All hyperspectral and multispectral line-scan imaging was conducted on a 140 birds/min chicken kill line at a Tyson Foods processing facility (Cumming, GA). Stage I hyperspectral imaging acquisition was conducted in March 2007. Stage II hyperspectral imaging acquisition, stage II multispectral on-line inspection (limited), and stage III multispectral on-line inspection (continuous inspection over 2 shifts) was conducted in July 2007.

Calibration of the transportable spectral line-scan imaging system was necessary at the start of each day's work after the equipment was put on the chicken processing line because the system was dismantled and removed at the end of each day. A white 99% diffuse reflectance panel was used as a reference target while the LED line lights were adjusted to maximize reflectance intensity across all pixels of the line-scan images. The target was mounted on a tripod positioned at a distance matching the chicken-to-lens distance used during on-line imaging. Following the illumination adjustment, white ($\boldsymbol{W}$) and dark ($\boldsymbol{D}$) reference images were acquired. Five line-scan images were acquired using the illuminated reference target; these were averaged to calculate the reference image W. With the lights off and the camera lens covered, another 5 line-scan images were acquired and averaged to calculate the reference D. The reference images W and D were used by the software of the imaging system during on-line imaging to convert raw reflectance line-scan images (I_0) that were subsequently acquired that day to relative reflectance line-scan images (I), according to the following equation: $I = (I_0 - D)/(W - D)$.

Stage I: Development

Conducting continuous line-scan imaging of birds on a moving processing line required the development of a bird detection algorithm. Once it is turned on, the spectral line-scan imaging system continuously acquires line-scan images regardless of what is presented in its FOV, and no external sensors are used to tell the system whether a bird is present or not. Thus, a bird detection algorithm was developed for real-time analysis of each individual line-scan image immediately after

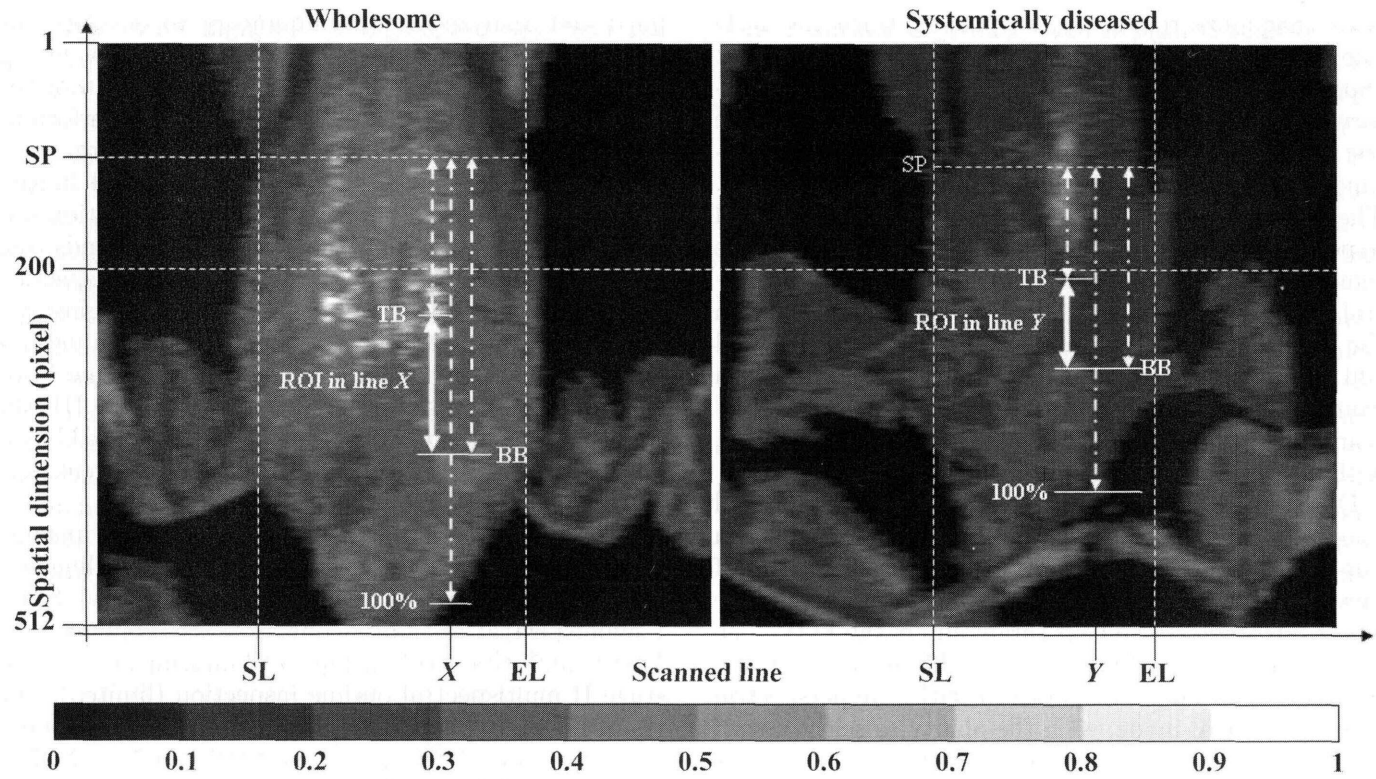

Figure 2. Reference points defining the possible region of interest (ROI) areas for analysis: the starting point (SP), the starting line (SL), the ending line (EL), the top boundary (TB), and the bottom boundary (BB).

acquisition, to enable the system to detect the entry and exit of individual birds in the FOV. During all on-line imaging of birds on the processing line, a black panel was hung behind the processing line, opposite the imaging system, for image segmentation (i.e., to enable separation of bird carcass pixels from background pixels in the images).

Stage I hyperspectral imaging was conducted to collect line-scan images for the off-line analysis used to develop the bird detection algorithm. The system was freely run to acquire hyperspectral line-scan images of birds on the processing line, with a veterinarian posted beside the imaging system to observe and evaluate each bird's condition. Hyperspectral line-scan images were recorded for a total of 5,309 birds (5,260 wholesome, 49 systemically diseased) during stage 1 hyperspectral imaging.

Bird Detection Algorithm. Figure 2 shows the 620-nm waveband for 2 whole-carcass bird images compiled from hyperspectral line-scan images. Analysis of the hyperspectral data found that carcass pixels and background pixels showed the greatest difference in relative reflectance at the 620-nm waveband. Therefore, a threshold value of 0.1 relative reflectance intensity at 620 nm was selected by which the bird detection algorithm could classify pixels as being either carcass pixels (intensity $\geq$0.1) or background (intensity $<$0.1). Designed as a line-by-line algorithm for on-line imaging, the bird detection algorithm examines the relative reflectance at the 620-nm waveband in each new line-scan image acquired.

The bird detection algorithm examines only the upper 200 pixels in each line-scan image, corresponding to the uppermost 69 mm of the FOV, covering the height at which a properly hung bird's legs would appear in the FOV. This upper area of the line-scan image was termed the carcass detection length (**CDL**). If all CDL pixels showed 620-nm relative reflectance values below the 0.1 threshold, the algorithm assumes that no bird is present in the FOV. The initial entry of a bird into the FOV is recognized when the relative reflectance at 620 nm increases above the 0.1 threshold for any single pixel within the 200 CDL pixels (i.e., the detection of a nonbackground pixel). This method only examines the uppermost 200 pixels to disregard possible anomalies in the position of the wings. After the initial detection of a nonbackground pixel in the CDL, each subsequent line-scan image is monitored for the appearance of additional nonbackground pixels in the CDL. As a bird continues to move across the FOV, the bird's leg and body begin to fill the area of the CDL pixels. Eventually, the algorithm finds a line-scan image containing only one remaining background pixel or several adjacent background pixels in the CDL, immediately followed by a line-scan image containing no background pixels. When this occurs, the spatial coordinate of the last background pixel is recorded, and the pixel at this same coordinate in the line scan that contains no background pixels is identified as the starting point (**SP**) for the bird. This point is located along the leading edge of the chicken at the junction of the thigh and the side of the belly, as shown in Figure 2. The line-scan image

containing this SP pixel is identified as the starting line (**SL**) for the bird. The bird detection algorithm continues to monitor the pixels in subsequent line-scan images that are located at the same SP coordinate until those pixels indicate a turnover in 620-nm relative reflectance intensity from nonbackground ($\geq$0.1) back to background (<0.1). This turnover indicates that the main body of the bird has passed through the FOV and that the ending line (**EL**) of the bird has been found. The SP, SL, and EL are marked on the 2 example bird images in Figure 2.

Region of Interest Selection. The line-by-line bird detection algorithm described above was the critical framework on which the differentiation method to identify wholesome and systemically diseased birds on-line was developed. For each bird, differentiation was based only on analysis of breast-area pixels located within the line-scan images between the SL and EL, avoiding irregularly illuminated areas such as the wings, legs, and sides of the body. However, even between the SL and EL, analysis of all of the pixels in these line-scan images was not desirable due to variations in bird size and shape, which caused some birds to have many background pixels showing at the bottom of each line scan and shadow-edge effects, whereas other birds might have no such pixels, which could also produce some shadow effects along the edges of the breast area. It was thus necessary to select a region of interest (**ROI**) in each line-scan image containing pixels to be analyzed for bird differentiation.

Already identified by the bird detection algorithm, the SP was an important reference point for locating the boundaries of potential ROI on the bird breast area to be used for effective differentiation. Figure 2 shows the reference points used to define the possible ROI areas. Within each line-scan image between a bird's SL and EL, possible ROI pixels were counted starting from the pixel at the SP coordinate (0%) and proceeding down to either the first background pixel encountered toward the bottom of the line-scan image or the last nonbackground pixel if no background pixels were present at the bottom of the line-scan image (100%). The ROI investigated for ROI selection were defined by a top boundary (**TB**) value and a bottom boundary (**BB**) value, each of which specifies a percentage of the full 100% possible ROI region. For example, for an ROI defined by a TB value of 30% and BB value of 70%, each line scan between the SL and EL would be examined to find the location of the bottommost pixel that defines the 100% ROI, and the pixels located from the 30% location down to the 70% location would be selected for analysis as ROI pixels. Regions of interest defined by TB values of 10, 20, 30, and 40% and BB values of 60, 70, 80, and 90% were evaluated as described below to select ROI boundaries for effective differentiation of wholesome and systemically diseased chickens.

For each potential ROI as defined by specific TB and BB values, ROI pixels were extracted from the hyperspectral images of 785 wholesome chickens and the spectra of all of these pixels were averaged to calculate the average wholesome ROI spectrum. Similarly, the average systemically diseased ROI spectrum was calculated using ROI pixels extracted from the hyperspectral images of 9 systemically diseased chickens. For each potential ROI, the difference spectrum (between the average wholesome and average systemically diseased spectra) was calculated. Maxima points in the difference spectrum show the wavelengths at which wholesome and systemically diseased spectra differ the most in their spectral character. By evaluating the potential ROI in this manner, the final ROI selection was that which produced the greatest magnitude spectral differences between wholesome and systemically diseased spectra.

Waveband Selection. Given the final selection of ROI boundaries to use, a bird differentiation algorithm was then developed to identify wholesome and systemically diseased birds based on ROI pixel analysis using 1) relative reflectance intensity measured at a single waveband and 2) a ratio of the relative reflectance intensities measured at 2 different wavebands.

To select a single waveband for use in intensity-based differentiation, the difference spectrum was calculated between the average wholesome ROI spectrum and average systemically diseased ROI spectrum. The single waveband at which the greatest difference occurred was selected as key waveband A (i.e., the intensity at A for each individual ROI pixel of a bird ($\boldsymbol{I_A}$) would be used as an input feature to the multispectral differentiation algorithm). From the hyperspectral data set of 785 wholesome and 9 systemically diseased birds, the average and SD values of I_A were also calculated for all of the wholesome ROI pixels and all of the systemically diseased ROI pixels, to be used as inputs to the multispectral differentiation algorithm.

To select a pair of wavebands for use in 2-waveband ratio-based differentiation, wavebands were identified at 3 local maximum points in the average wholesome and average systemically diseased ROI pixel spectra; each of these peak wavebands was paired with a base waveband at a local minimum point preceding the peak. For each peak-base waveband pair, the ratio of the 2 waveband intensities was calculated for the average wholesome ROI pixel spectrum, and also for the average systemically diseased ROI pixel spectrum. The difference between the wholesome ratio value and systemically diseased ratio value was then calculated for each peak-base pair. The pair that produced the greatest difference between the wholesome ratio value and the systemically diseased ratio value was selected to be used for ratio-based differentiation, with the peak waveband identified as p and its paired base waveband identified as b. Thus, the ratio of the intensities at b and p for an individual ROI pixel ($\boldsymbol{I_b{:}I_p}$) would be used as an input feature to the multispectral differentiation algorithm. The average and SD values for the wholesome $I_b{:}I_p$ ratio and for the systemically diseased $I_b{:}I_p$

ratio were also calculated from the hyperspectral data set to be used as inputs to the multispectral differentiation algorithm.

Multispectral Differentiation Algorithm. The multispectral differentiation algorithm was built around the line-by-line bird detection algorithm and was developed to incorporate the I_A values and I_b:I_p ratio values for individual ROI pixels as initial input features. A method to analyze individual pixels as being indicative of systemic disease was developed using 2 mapping functions, one for intensity differentiation and another for ratio differentiation. The differentiation algorithm first calculates outputs for each ROI pixel of an individual bird and then calculates a final output value for the bird based on the pixel outputs.

To calculate outputs for an ROI pixel, the mapping functions each convert one input value to one output value that estimates a pixel's possibility of being indicative of systemic disease, using 2 main reference points: 1) the average value of the input feature for systemically diseased ROI pixels and 2) the difference between the average and SD values of the input feature for wholesome ROI pixels. Figure 3 shows the intensity-differentiation mapping function and ratio-differentiation mapping function, where reference points a, b, c, and d are defined as follows: a = the average I_A for systemically diseased ROI pixels; b = the difference between average I_A and its SD for wholesome ROI pixels; c = the average I_b:I_p for systemically diseased ROI pixels; and d = the difference between average I_b:I_p and its SD for wholesome ROI pixels.

The intensity differentiation mapping function assigned the intensity output ($\boldsymbol{O_I}$) to be 1 when the input $I_A \leq a$ and to be 0 when the input $I_A \geq b$. For input values between a and b, output O_I was calculated according to this formula: $O_I = (b - I_A)/(b - a)$. Similarly, the ratio differentiation mapping function assigned the ratio output ($\boldsymbol{O_R}$) to be 1 when the input I_b:$I_p \leq c$ and to be 0 when the input I_b:$I_p \geq d$. For input values between c and d, output O_R was calculated according to this formula: $O_R = (d - I_b{:}I_p)/(d - c)$. Higher output values were correlated to a higher possibility of a pixel being indicative of systemic disease.

The multispectral differentiation algorithm begins for a single bird when the bird detection algorithm first detects the SP and the SL (i.e., when the system knows there is a bird present and ready to be analyzed). Once the SL is detected, the ROI pixels within this line-scan image are immediately located. For each ROI pixel, the I_A, I_p, and I_b values are acquired, the I_b:I_p ratio is calculated, and the O_I and O_R values are immediately calculated. For each ROI pixel, the O_I and O_R values are averaged to produce one output value for each ROI pixel ($\boldsymbol{O_{pixel}}$), and this value is temporarily stored in memory as line-scan imaging continues. For each new line-scan image, this same process of immediately locating ROI pixels and calculating O_{pixel} for each pixel is repeated until the bird detection algorithm detects the EL, which indicates that there are no more relevant line-scan images to analyze for the current bird. At this point, the algorithm has temporarily stored an O_{pixel} value for every ROI pixel for the bird and now calculates the average O_{pixel} value for all ROI pixels. This final averaged decision output ($\boldsymbol{O_f}$) is compared with a preset threshold value ($\boldsymbol{T}$) to identify the bird as being either wholesome or systemically diseased: if $O_f \geq T$, bird is systemically diseased and if $O_f < T$, bird is wholesome.

After the final classification of a bird as either systemically diseased or wholesome, the algorithm begins again to analyze subsequent line-scan images to detect the SP of the next bird to be inspected.

Off-Line Multispectral Differentiation. The multispectral inspection algorithm was tested using the remaining hyperspectral images of 4,475 wholesome and 40 systemically diseased birds that were not used during analysis and development of the inspection algorithm. Although the images consisted of hyperspectral data (55 spectral channels), testing used only I_A, I_p, and I_b, the intensities at the key waveband A and at the peak and base wavebands, during off-line execution of the line-by-line multispectral inspection algorithm.

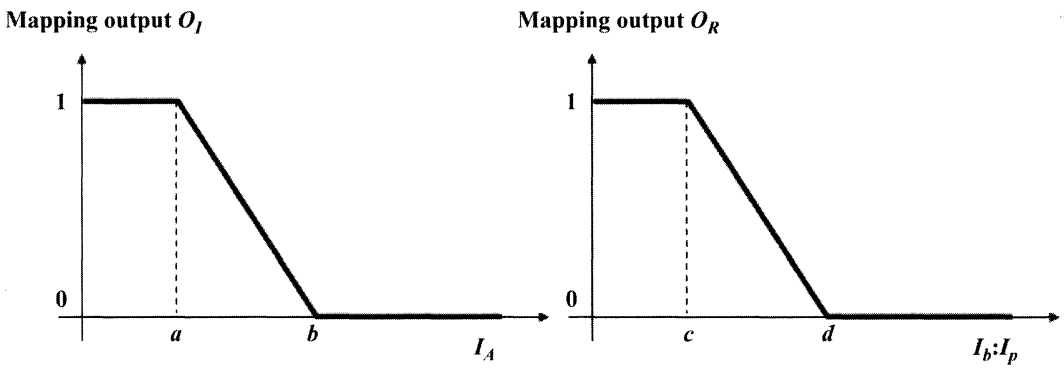

Figure 3. The structure of the intensity-differentiation and ratio-differentiation mapping functions used to convert I_A and I_b:I_p inputs to outputs O_I and O_R, respectively. I_A = the intensity at A for each individual region of interest (ROI) pixel of a bird, where A is the single waveband at which the greatest difference occurred; I_b:I_p = ratio of the intensities at b and p for an individual ROI pixel, where p is the peak waveband and b is its paired base waveband; O_I = intensity output; O_R = ratio output.

Stage II: Validation

ROI and Waveband Selection. In stage II, the ROI and waveband selections that were used to develop the multispectral inspection algorithm were validated. For this purpose, a new set of hyperspectral images was acquired for 191 wholesome chickens and 7 systemically diseased chickens on the 140 birds/min processing line. The process of evaluating ROI and selecting wavebands used in stage I was repeated using this new hyperspectral image data.

On-Line Multispectral Inspection Validation by Veterinarian. The multispectral inspection algorithm was tested on-line with the assistance of an FSIS veterinary medical officer. The imaging system was set up for multispectral imaging on the 140 birds/min processing line and the veterinarian was posted beside the imaging system to observe the birds in real time, immediately before they entered the imaging FOV. The veterinarian identified systemically diseased birds, and the classification decision of the imaging system for each of these birds was compared with the veterinarian's identification. Because of the low-frequency occurrence of systemically diseased birds, on-line multispectral inspection in this manner was conducted during 2-d shifts to obtain a total data set of 90 systemically diseased chickens.

Stage III: On-Line System Evaluation

In stage III, the performance of the imaging system was evaluated based on continuous multispectral inspection of chickens on the processing line during two 8-h shifts in the processing plant. Because immediate comparison between inspection system output and inspector evaluations for individual birds was not feasible, the resulting counts of wholesome and systemically diseased birds produced by the inspection system were compared with numbers from the FSIS tally sheets produced by the human inspectors that worked the same processing line during those two 8-h shifts. Additionally, several limited periods (30 to 40 min each) of inspection verification were performed by a veterinarian who identified individual wholesome and systemically diseased chickens immediately before they entered the inspection system FOV, to produce direct comparison data for verification of the inspection system performance.

RESULTS AND DISCUSSION

Stage I: Development

ROI Selection. Hyperspectral images of 785 wholesome chickens and 9 systemically diseased chickens were analyzed to select an ROI for use by the differentiation algorithm. Sixteen possible ROI were considered, defined by TB values of 10, 20, 30, and 40% and BB values of 60, 70, 80, and 90%. The difference spectrum, calculated from the average wholesome ROI pixel spectrum and average systemically diseased ROI pixel spectrum, consisted of the average intensity difference at each of 55 spectral channels; the range of these values for each of the possible ROI is shown in Figure 4. For example, for the 10 to 90% ROI, the greatest intensity difference between wholesome and systemically diseased chickens was 0.195 (occurring at the 580-nm spectral channel), and the lowest intensity difference was 0.153 (occurring at the 389-nm spectral channel). Between different ROI, individual spectral channels produced similarly distributed intensity differences; for example, the maximum intensity difference for each ROI was always produced by either the 573- or 580-nm spectral channel, and the minimum intensity difference always produced by the 389-nm spectral channel. However, the greatest magnitude single-channel intensity difference was 0.210 and occurred at the 580-nm spectral channel for the 40 to 60% ROI, represented at the top of the rightmost bar in Figure 4. For this reason, the 40 to 60% ROI was selected by which to differentiate wholesome and systemically diseased chickens.

Waveband Selection. Figure 5 shows the average wholesome ROI pixel spectrum and the average systemically diseased ROI pixel spectrum for pixels extracted from the 40 to 60% ROI. Because the greatest intensity difference occurs at 580 nm, this waveband was selected to be key waveband A for intensity-based differentiation. Figure 5 also shows the 3 peak wavebands and 3 base wavebands that were paired for use in 2-waveband ratio-based differentiation. For pair 1, the ratio of intensities at 435 and 455 nm was calculated first from the wholesome spectrum and then from the systemically diseased spectrum; the difference between the 2 ratio values was 0.003. For pair 2, using 495 and 534 nm, the difference between the 2 ratio values was 0.039. For pair 3, using 580 and 620 nm, the difference between the ratio values was 0.121. Pair 3 clearly results in a much greater difference in ratio values between the wholesome and systemically diseased spectrum. Thus, the 580- and 620-nm wavebands were selected as the base and peak wavebands, b and p, for differentiation of wholesome and systemically diseased birds using the ratio of the 2 waveband intensities, I_b:I_p.

Multispectral Differentiation Algorithm. The mapping functions used to classify ROI pixels as either wholesome or systemically diseased used the average and SD values for I_A and for I_b:I_p calculated from ROI pixels from the 785 wholesome and 9 systemically diseased chicken images. The average wholesome I_A value was 0.460 and the SD was 0.101. The average systemically diseased I_A value was 0.250 and the SD was 0.095. The mapping function for intensity-based pixel differentiation thus used reference point $a = 0.250$ (average systemically diseased I_A) and $b = 0.359$ (difference between the average wholesome I_A and the SD, $0.460 - 0.101$), shown in Figure 6.

Two-waveband ratio-based differentiation used the intensities at peak waveband $p = 620$ nm and base

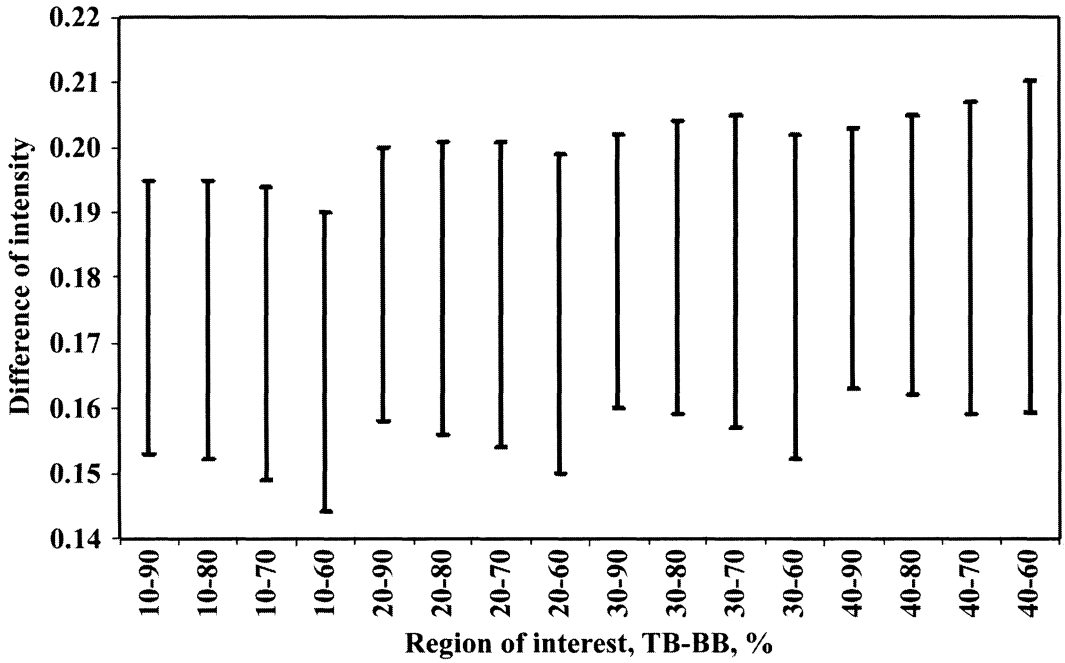

Figure 4. The range of the 55-channel spectral differences between the average wholesome region of interest (ROI) pixel spectrum and the average systemically diseased ROI pixel spectrum for each of 16 possible ROI. TB = top boundary; BB = bottom boundary.

waveband b = 580 nm. The average wholesome I_b:I_p value was 0.970 and the SD was 0.028. The average systemically diseased I_b:I_p value was 0.849 and 0.078. The mapping function for ratio-based pixel differentiation thus used reference points c = 0.849 (average systemically diseased I_b:I_p) and d = 0.942 (difference between the average wholesome I_b:I_p and the SD, 0.970 − 0.028), also shown in Figure 6.

Off-Line Multispectral Differentiation. The multispectral inspection algorithm utilizing the intensity-based differentiation and ratio-based differentiation inputs was tested off-line for hyperspectral images of

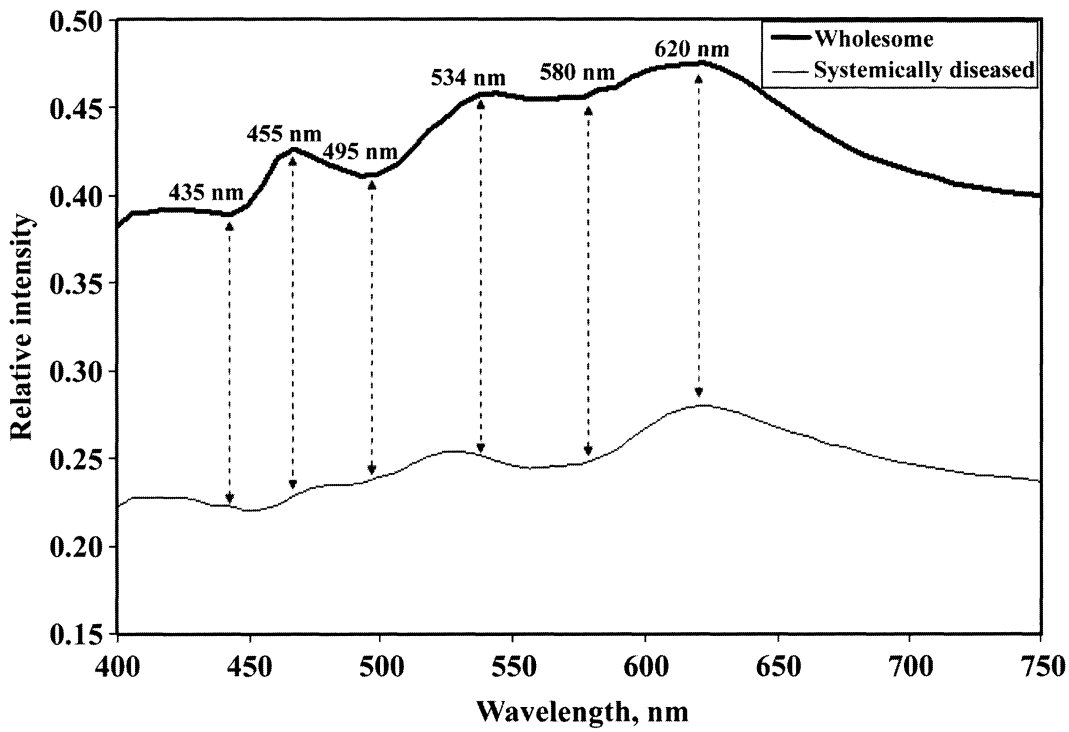

Figure 5. The average wholesome region of interest (ROI) pixel spectrum and average systemically diseased ROI pixel spectrum for pixels extracted from stage I hyperspectral images using the 40 to 60% ROI.

Table 1. Confusion matrix for off-line testing of differentiation algorithm for hyperspectral chicken images acquired during stage I algorithm development

	Machine system	
Veterinarian	Wholesome	Systemically diseased
Wholesome	4,474	1
Systemically diseased	2	38

4,475 wholesome and 40 systemically diseased chickens previously acquired, extracting only the data for the wavebands A, p, and b. Table 1 shows the confusion matrix for the results: the system correctly identified 4,474 of 4,475 wholesome chickens and 38 of 40 systemically diseased chickens. Figure 7 shows the distribution of the inspection system results, where the O_f decision output value falls above the threshold value $T = 0.60$ for all but 2 systemically diseased chickens and also for one of the 4,475 wholesome chickens.

Stage II: Validation

The process of evaluating ROI and waveband selections was repeated using a new set of hyperspectral images acquired for 191 wholesome chickens and 7 systemically diseased chickens on the 140 birds/min processing line. The new hyperspectral images were acquired on-line with the use of an FSIS-approved motor-driven guiding belt installed behind the chicken carcasses. During stage I imaging, it was observed that chicken carcasses hung on the shackles were often subject to a swinging motion that could increase inconsistency in the distance from carcass to lens. To address this concern, the guiding belt was installed in stage II to operate in synchronization with the processing line so as to provide physical support from behind the chickens without creating drag or otherwise interfering in movement along the line. The belt minimized carcass vibration and increased the consistency of the focal distance. The belt primarily contacted the thigh and leg area of a wholesome bird.

Using the newly acquired hyperspectral data, the evaluation of 16 possible ROI again found that the 40 to 60% ROI yielded the greatest single-channel difference (0.167) between the average wholesome ROI pixel spectra and the average systemically diseased ROI pixel spectrum, again occurring at the 580-nm waveband. This waveband confirmed the 580-nm waveband as key waveband A for intensity-based differentiation, with an average I_A of 0.392 for wholesome ROI pixels and SD of 0.102 and an average I_A of 0.225 for systemically diseased ROI pixels and SD of 0.074. For 2-waveband ratio-based differentiation, the same 3 waveband pairs were evaluated: For pair 1, using 435 and 455 nm, the difference between the wholesome and systemically diseased ratio values was 0.029. For pair 2, using 495 and 534 nm, the difference between the 2 ratio values was 0.030. For pair 3, using 580 and 620 nm, the difference between the ratio values was 0.044. Thus, the 580- and 620-nm wavebands were confirmed as the selections for the base and peak wavebands, b and p, for differentiation of wholesome and systemically diseased birds using the I_b:I_p ratio of the 2 waveband intensities. The average I_b:I_p for wholesome ROI pixels in the hyperspectral data set was 0.948, with a SD of 0.036. The average I_b:I_p for systemically diseased ROI pixels was 0.904, with a SD of 0.052.

From these results, the new mapping function reference points were assigned as $a = 0.225$; $b = 0.290$; $c = 0.904$; and $d = 0.912$. Multispectral on-line inspection was conducted to test the multispectral inspection algorithm with these new reference points. The veterinarian identified systemically diseased birds approaching the inspection system and the classification identification decisions of the inspection system for

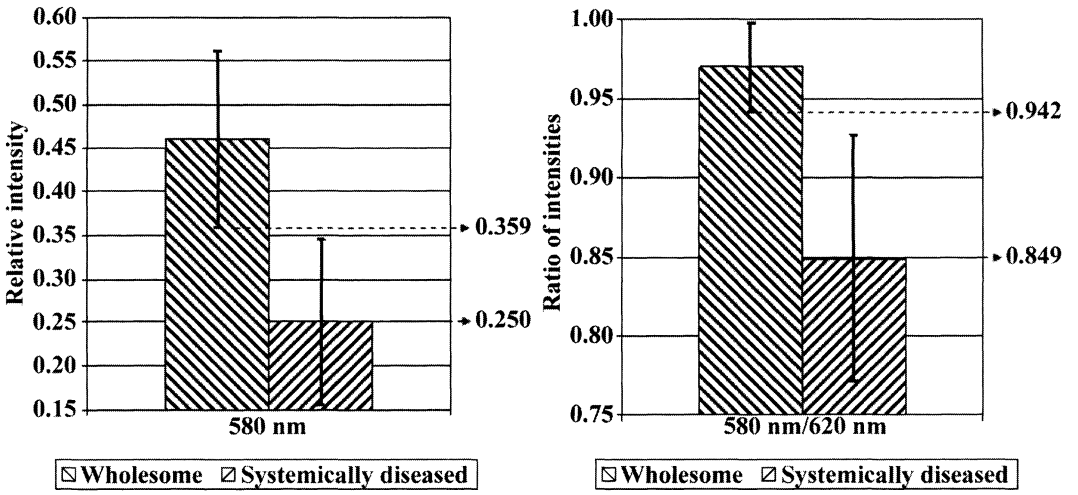

Figure 6. The average and SD values for I_A and I_b:I_p for region of interest (ROI) pixels from stage I hyperspectral images, for A = 580 nm, b = 580 nm, and p = 620 nm. I_A = the intensity at A for each individual ROI pixel of a bird; I_b:I_p = ratio of the intensities at b and p for an individual ROI pixel.

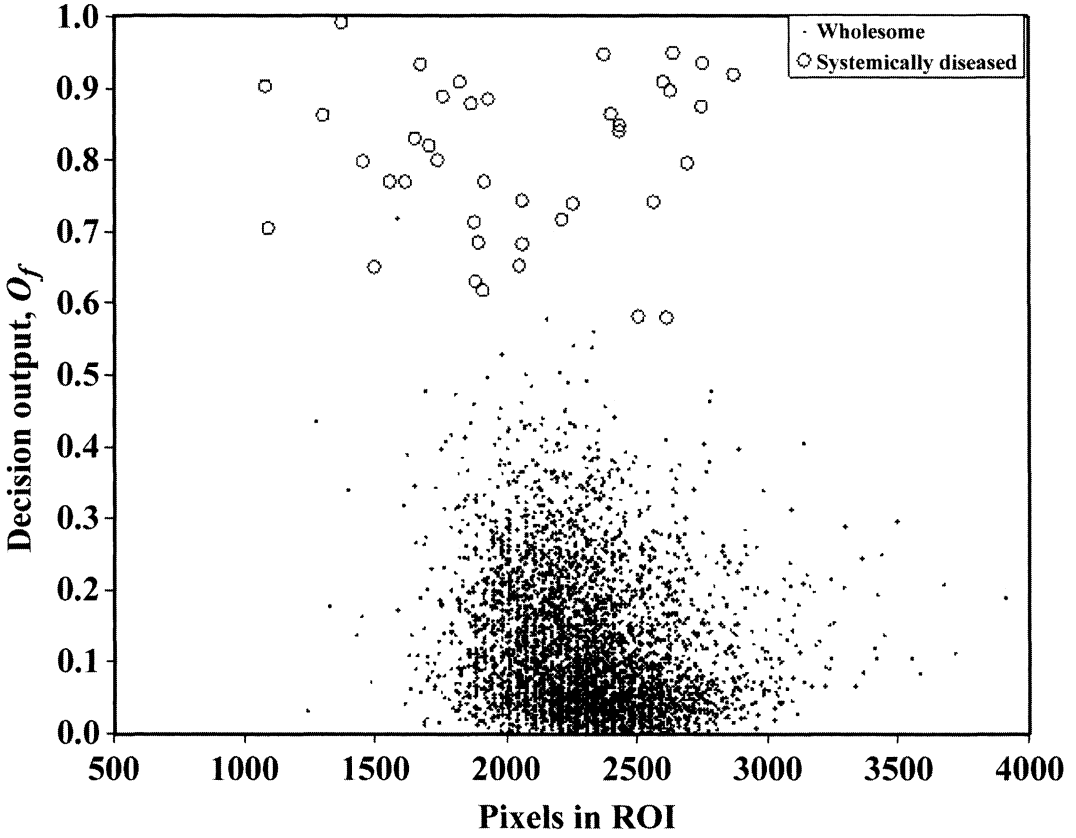

Figure 7. The inspection system results for off-line multispectral differentiation of stage I hyperspectral images. ROI = region of interest.

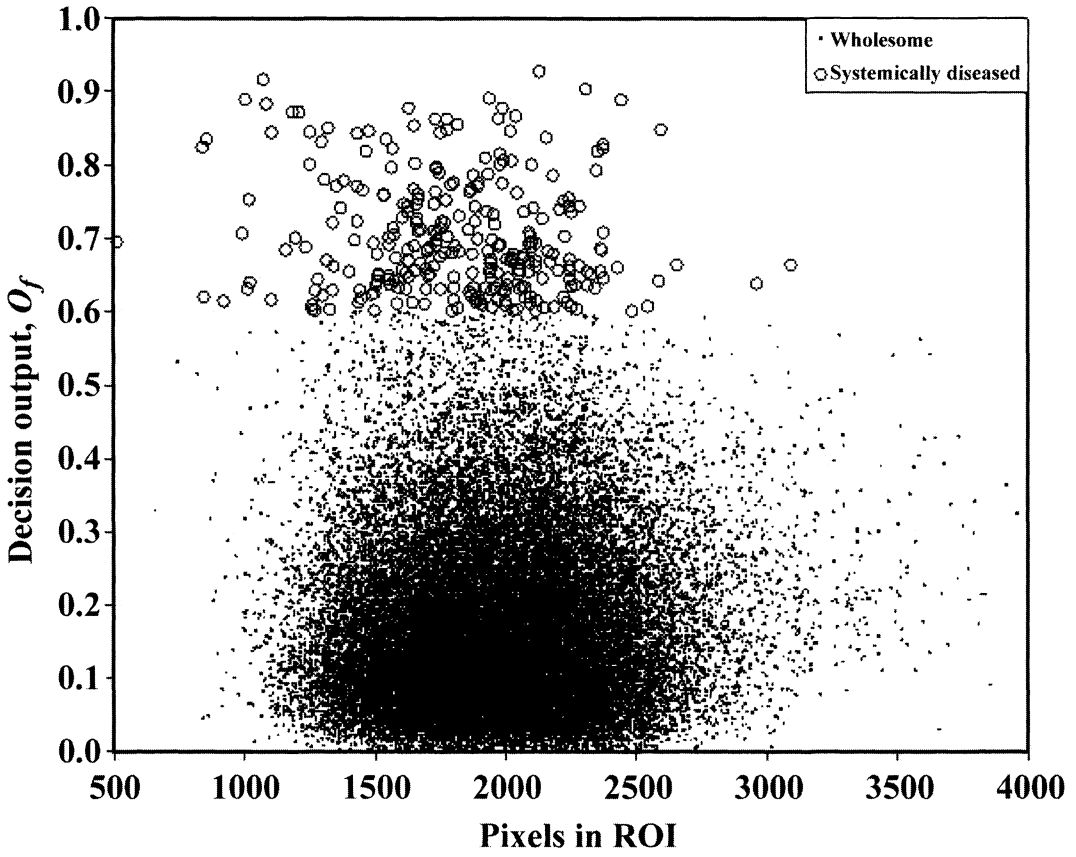

Figure 8. The inspection system results for on-line multispectral inspection of chickens on the processing line during stage III, shift 1. ROI = region of interest.

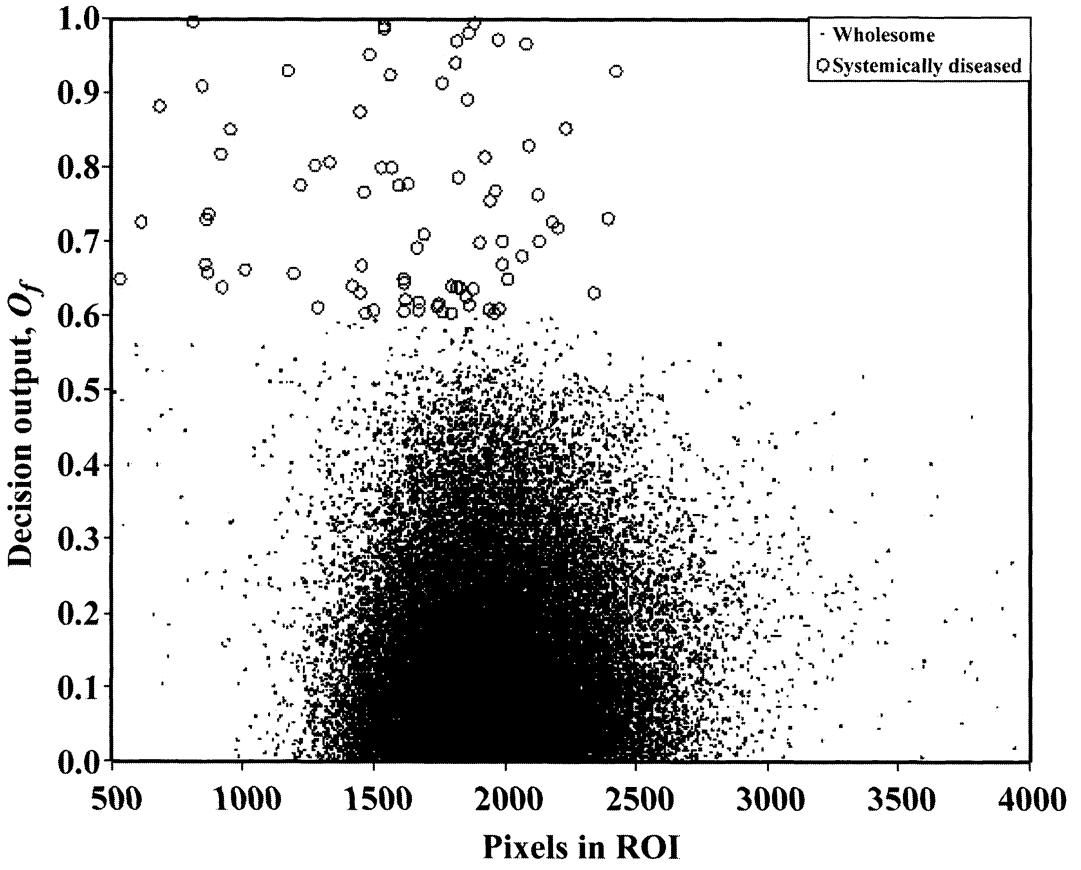

Figure 9. The inspection system results for on-line multispectral inspection of chickens on the processing line during stage III, shift 2. ROI = region of interest.

these specific birds were immediately compared with the veterinarian's diagnosis. Again, the low-frequency occurrence of systemically diseased birds required on-line multispectral inspection to be conducted during 2-d shifts to obtain a total data set of 90 systemically diseased chickens. The O_f value for each of the 90 birds fell above the 0.60 threshold value; thus, the machine correctly classified 100% of these 90 systemically diseased birds.

Stage III: On-Line System Evaluation

With finalization of the intensity- and ratio-based reference points for the differentiation algorithm, the multispectral inspection system was tested on the poultry processing line during the operation of 2 normal 8-h day shifts. Due to logistical requirements with plant operations, the system was allowed to be set up on the line and turned on only after the processing line had already begun to move at the start of each shift, and the system was required to be disassembled and removed before final washdown, which was immediately begun on the tails of the last bird on the processing line during the day shift. Consequently, the system was tested during continuous operation over most of the duration of each day shift but was not able to inspect all of the birds processed during that shift.

Table 2. Confusion matrix for verification of inspection system results during shift 1 on-line multispectral inspection by veterinarian identifications

	Machine system	
Veterinarian	Wholesome	Systemically diseased
Wholesome	16,056	118
Systemically diseased	2	41

During the first shift, the inspection system identified 254 of 45,456 chickens as being systemically diseased, indicating a systemically diseased fraction of 0.56%. The FSIS tally sheets showed that inspectors counted 84 of 53,563 birds as being systemically diseased, a fraction of 0.16%. During the second shift, the inspection system identified 98 of 61,020 chickens as being systemically diseased, a systemically diseased fraction of 0.16%. The FSIS tally sheets showed that inspectors counted 71 of 64,971 birds as being systemically diseased, a fraction of 0.11%. Although bird-by-bird direct comparison of system and human inspectors was not feasible, the relative fractions of systemic bird identified by each side are similar, suggesting that the inspection system was operating in a consistent manner to identify systemically diseased birds. Figures 8 and 9 show the distribution of the O_f decision values for the first and second shifts, respectively, where all systemically

Table 3. Confusion matrix for verification of inspection system results during shift 2 on-line multispectral inspection by veterinarian identifications

	Machine system	
Veterinarian	Wholesome	Systemically diseased
Wholesome	27,580	46
Systemically diseased	1	34

diseased decision outputs are above $T = 0.6$. It can be observed that the bird detection and multispectral inspection algorithms detected and analyzed between 500 and 4,000 ROI pixels per bird, depending on the size of the bird. Although systemically diseased birds exhibit a general tendency to be smaller than wholesome birds, the distribution shows that the inspection system did not assume smaller birds to be systemically diseased, and a sufficient number of ROI pixels were detected even for the smallest birds for effective inspection.

System verification was also performed during multiple periods of 30 to 40 min, during which identification of birds by a veterinarian posted beside the inspection system could be directly compared with the inspection system's final output for each bird. During the first shift, a total of 16,217 chickens were identified by the veterinarian before inspection over 4 verification periods; during the second shift, a total of 27,661 chickens were identified before inspection. Tables 2 and 3 show the confusion matrices to compare veterinarian identification with inspection system output for these birds. The system correctly identified 99.3 and 99.8% of wholesome chickens during the shift 1 and shift 2 verification periods, respectively, and correctly identified 95.4 and 97.1% of systemically diseased chickens during those same verification periods. These results, combined with the general performance of the system as considered against FSIS tally sheets, demonstrates that the inspection system can effectively classify wholesome and systemically diseased chickens on a 140 birds/min processing line. An ideal application for this system would be on-line presorting of young chickens on high-speed kill lines in a HIMP processing plant, using a conservative adjustment of the decision threshold to prevent unwholesome birds from entering the evisceration line. The much smaller fraction of unwholesome and questionable birds would be easily diverted to a rejection line that, if desired, could allow for reinspection by a human inspector to minimize possible economic losses posed by rejected wholesome birds.

In conclusion, a line-scan spectral imaging system successfully implemented a multispectral bird detection and inspection algorithm to differentiate systemically diseased chickens from wholesome chickens on a 140 birds/min high speed commercial processing line. The system successfully performed on-line hyperspectral image acquisition to collect data for development of a line-by-line multispectral bird detection and differentiation algorithm. The same system was then used for implementation of the multispectral differentiation algorithm, and demonstrated effective on-line multispectral inspection of chickens at 140 birds/min during in-plant testing conducted over two 8-h shifts. The system can be used for on-line inspection applications to increase efficiency, reduce labor and cost, and produce significant benefits for poultry processing plants.

REFERENCES

Chao, K., C. C. Yang, Y. R. Chen, M. S. Kim, and D. E. Chan. 2007. Hyperspectral-multispectral line-scan imaging system for automated poultry carcass inspection applications for food safety. Poult. Sci. 86:2450–2460.

Daley, W., D. Britton, J. Stewart, and C. Usher. 2003. Front to back: Applications of image processing in poultry processing. Proc. 26th Tech. Turkey Conf., Macclesfield, UK.

Lawrence, K. C., B. Park, W. R. Windham, and C. Mao. 2003a. Calibration of a pushbroom hyperspectral imaging system for agricultural inspection. Trans. ASAE 46:513–521.

Lawrence, K. C., W. R. Windham, B. Park, and R. J. Buhr. 2003b. A hyperspectral imaging system for identification of fecal and ingesta contamination on poultry carcasses. J. Near Infrared Spectrosc. 11:269–281.

Mehl, P. M., K. Chao, M. S. Kim, and Y. R. Chen. 2002. Detection of contamination on selected apple cultivars using reflectance hyperspectral and multispectral analysis. Appl. Eng. Agric. 18:219–226.

Park, B., and Y. R. Chen. 1996. Multispectral image co-occurrence matrix analysis for poultry carcass inspection. Trans. ASAE 39:1485–1491.

Park, B., K. C. Lawrence, W. R. Windham, and R. J. Buhr. 2002. Hyperspectral imaging for detecting fecal and ingesta contamination on poultry carcasses. Trans. ASAE 45:2017–2026.

USDA. 1996. Pathogen reduction: Hazard Analysis and Critical Control point (HACCP) systems: Final rule. Fed. Regist. 61:38805–38989.

USDA. 1997. HACCP-based inspection models project (HIMP): Proposed rule. Fed. Regist. 62:31553–31562.

USDA. 2009. Poultry—Production and Value, 2008 Summary. USDA, Washington, DC.

Usher, C., D. Britton, W. Daley, and J. Stewart. 2005. Machine vision process monitoring on a poultry processing kill line: Results from an implementation. SPIE Optics East, Boston, MA.

Windham, W. R., D. P. Smith, B. Park, K. C. Lawrence, and P. W. Feldner. 2003. Algorithm development with visible/near-infrared spectra for detection of poultry feces and ingesta. Trans. ASAE 46:1733–1738.

Yang, C. C., K. Chao, Y. R. Chen, and H. L. Early. 2005. Systemically diseased chicken identification using multispectral images and region of interest analysis. Comput. Electron. Agric. 49:255–271.

Yang, C. C., K. Chao, Y. R. Chen, M. S. Kim, and D. E. Chan. 2006a. Development of fuzzy logic-based differentiation algorithm and fast line-scan imaging system for chicken inspection. Biosys. Eng. 95:483–496.

Yang, C. C., K. Chao, Y. R. Chen, M. S. Kim, and H. L. Early. 2006b. Simple multispectral image analysis for systemically diseased chicken identification. Trans. ASAE 49:245–257.